Electronic Supplementary Information for:

Interlayer exciton emission in MoS_2/VOPc inorganic/organic van der Waals heterostructure

Yuhan Kong[a,b], Sk Md Obaidulla[b,f], Mohammad Rezwan Habib[b], Zukun Wang[c], Rong Wang[d], Yahya Khan[b], Haiming Zhu[c], Mingsheng Xu[b], Deren Yang[e]**

[a] Department of Polymer Science and Engineering, Zhejiang University, Hangzhou 310027, P. R. China

[b] State Key Laboratory of Silicon Materials, School of Micro-Nano Electronics, Zhejiang University, Hangzhou 310027, P. R. China

E-mail: msxu@zju.edu.cn (M. S. Xu)

[c] Department of Chemistry, Zhejiang University, Hangzhou 310027, P. R. China

[d] ZJU Hangzhou Global Sci & Technol Innovat Ctr, Adv Semicond Res Inst, Hangzhou 311215, P. R. China

[e] State Key Laboratory of Silicon Materials, School of Materials Science and Engineering, Zhejiang University, Hangzhou 310027, P. R. China

Email: mseyang@zju.edu.cn (D. R. Yang)

[f] Center of Excellence for Advanced Materials and Sensing Devices, Institute of Physics, Bijenička cesta 46, HR-10000 Zagreb, Croatia

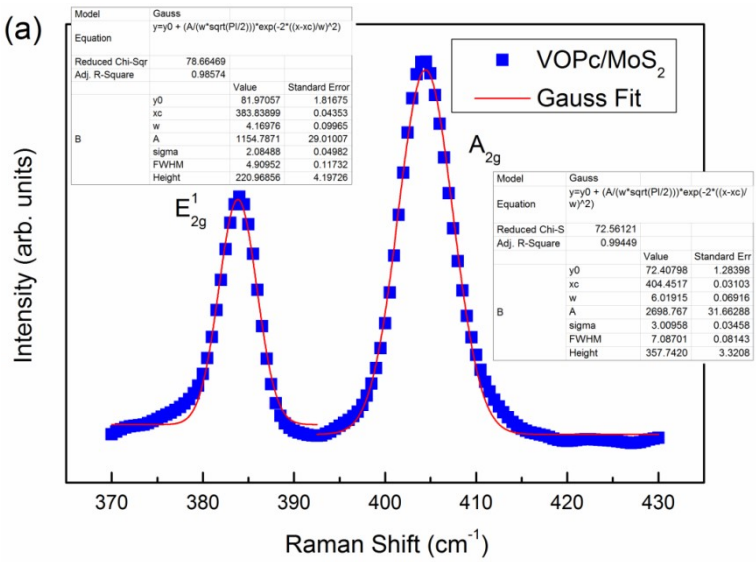

Figure S1. Gaussian fitting of Raman spectra of VOPc/MoS_2 heterostructure: the calculated full width at half maximum (FWHM) corresponding to E_{2g}^1 (386 cm-1) ~ 4.91 and A_{1g} (406 cm^{-1}) ~7.09, respectively.

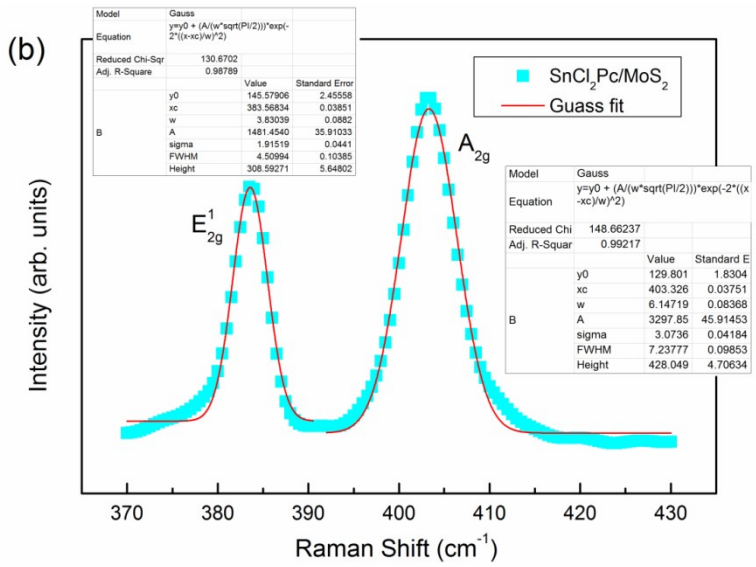

Figure S2. Gaussian fitting of Raman spectra of $SnCl_2Pc/MoS_2$ heterostructure: the calculated FWHM corresponding to E_{2g}^1 (386 cm-1) ~ 4.51 and A_{1g} (406 cm^{-1}) ~7.24, respectively.

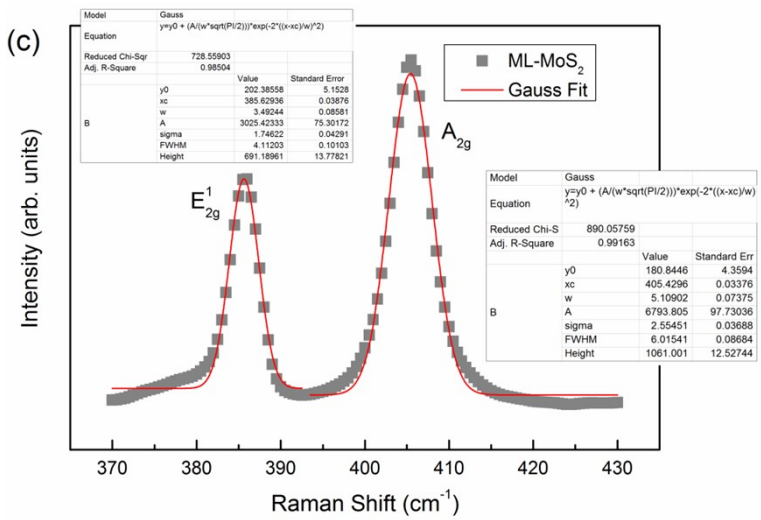

Figure S3. Gaussian fitting of Raman spectra of ML MoS_2, the calculated FWHM corresponding to E_{2g}^{1} (386 cm-1) ~ 4.11 and A_{1g} (406 cm^{-1}) ~6.02, respectively.

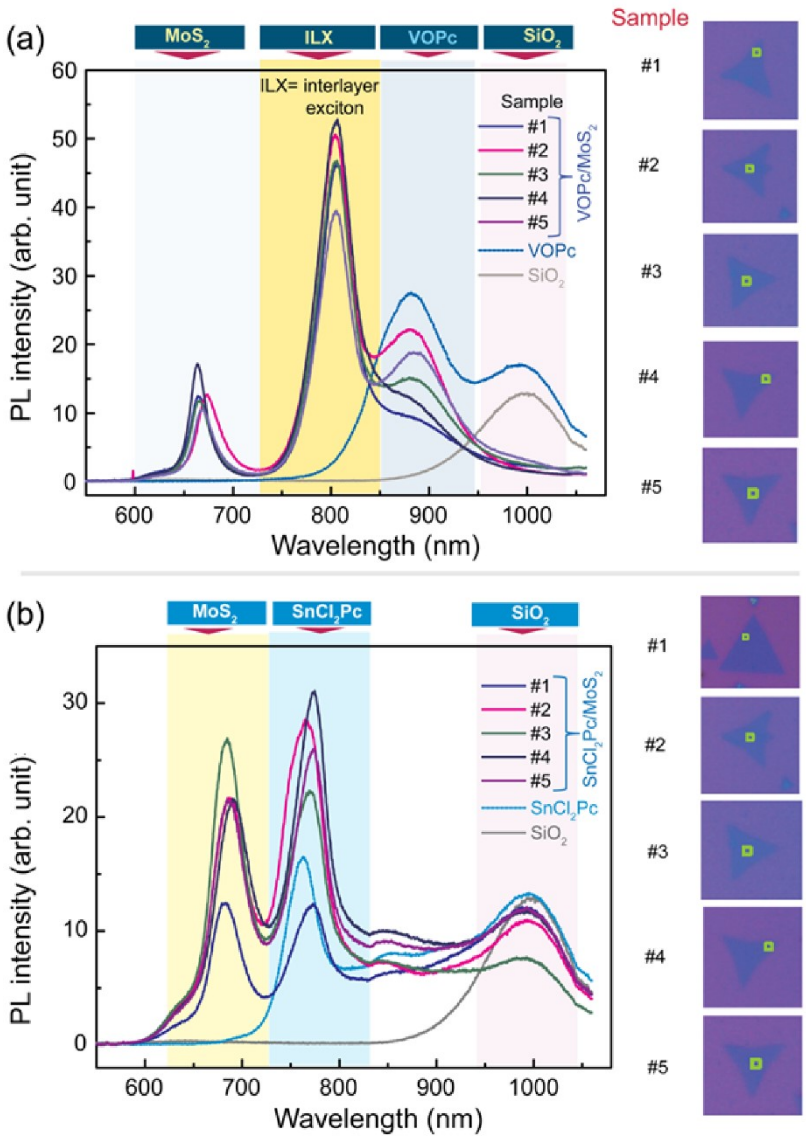

Figure S4. PL spectra (including individual constituent and sample background) of (a) VOPc/MoS_2 and (b) $SnCl_2Pc/MoS_2$ heterostructures and right side corresponding to 5 different samples.

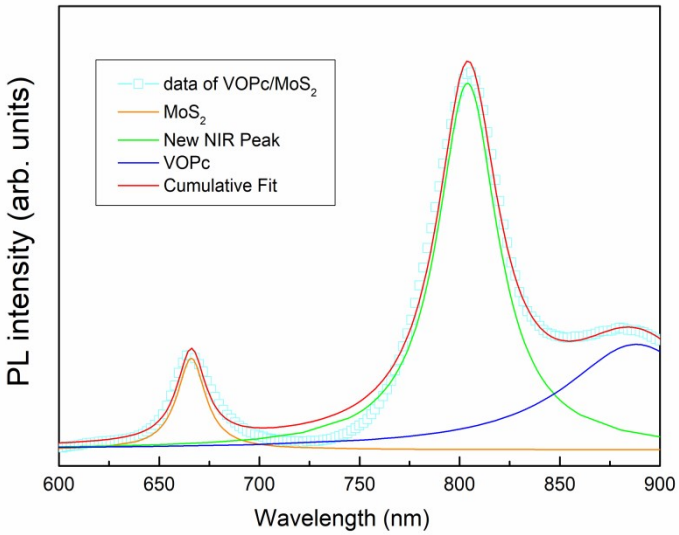

Figure S5. Peak fit of VOPc/MoS_2 heterostructure in which MoS_2 (668 nm), VOPc (880 nm), and the striking feature NIR emission peak at 805 nm (green line) are clearly resolved.

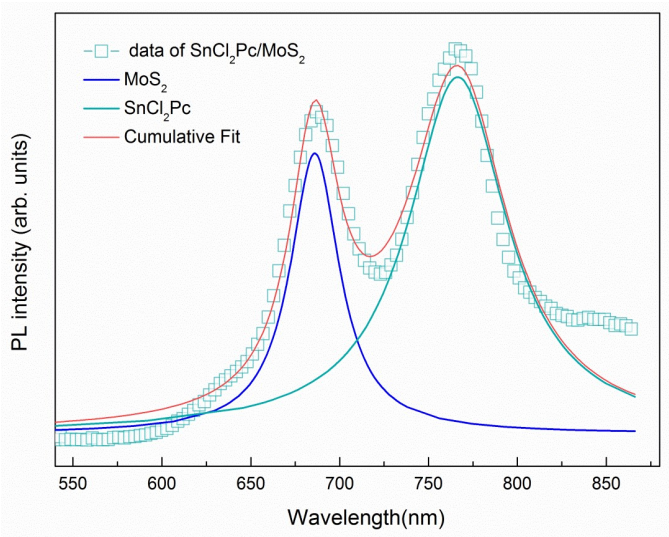

Figure S6. Peak fit of $SnCl_2Pc/MoS_2$ heterostructure in which MoS_2 (686 nm) and $SnCl_2Pc$ (766 nm) are clearly resolved.

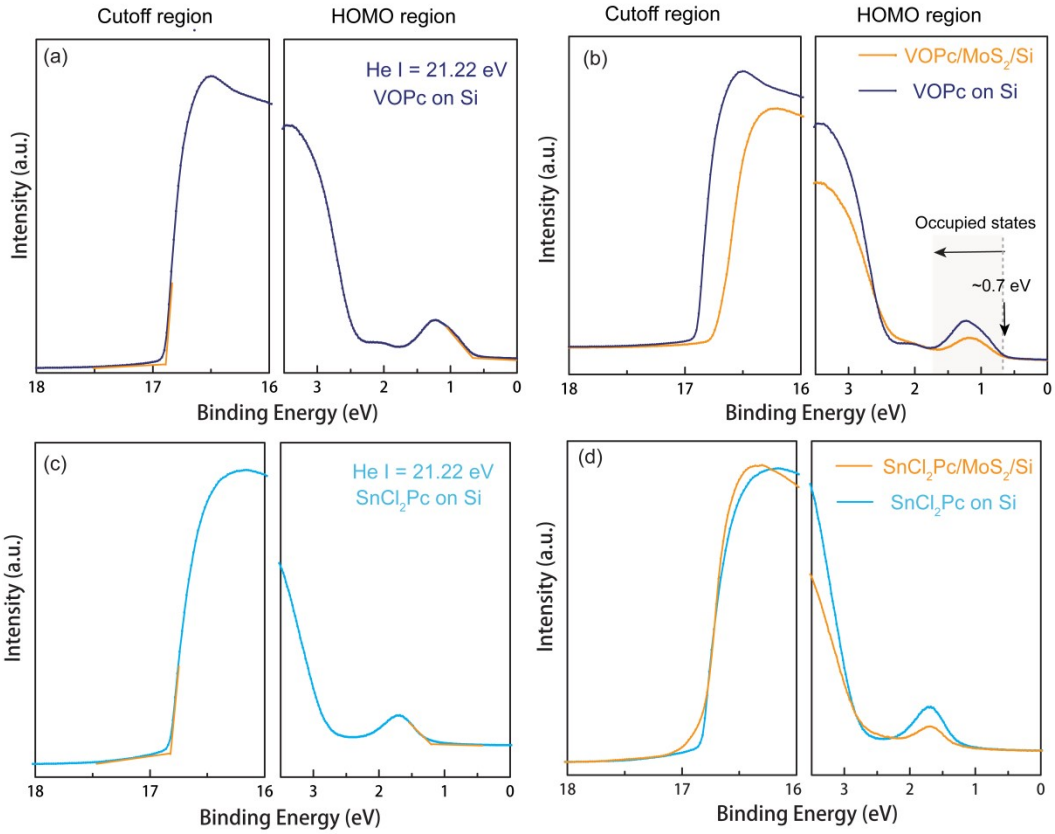

Figure S7. Ultraviolet photoelectron spectroscopy (UPS) spectrum (*hv* = 21.22 eV) (a,b) VOPc and VOPc/MoS_2 on pure highly doped Si substrate, (c,d) $SnCl_2Pc$ and $SnCl_2Pc/MoS_2$ on pure highly doped Si substrate. The thickness of organic thin films is about 5 nm. Please note that the MoS_2 was firstly synthesized on SiO_2 surface and then transfer to Si substrate for fabricating heterostructures for UPS measurement.

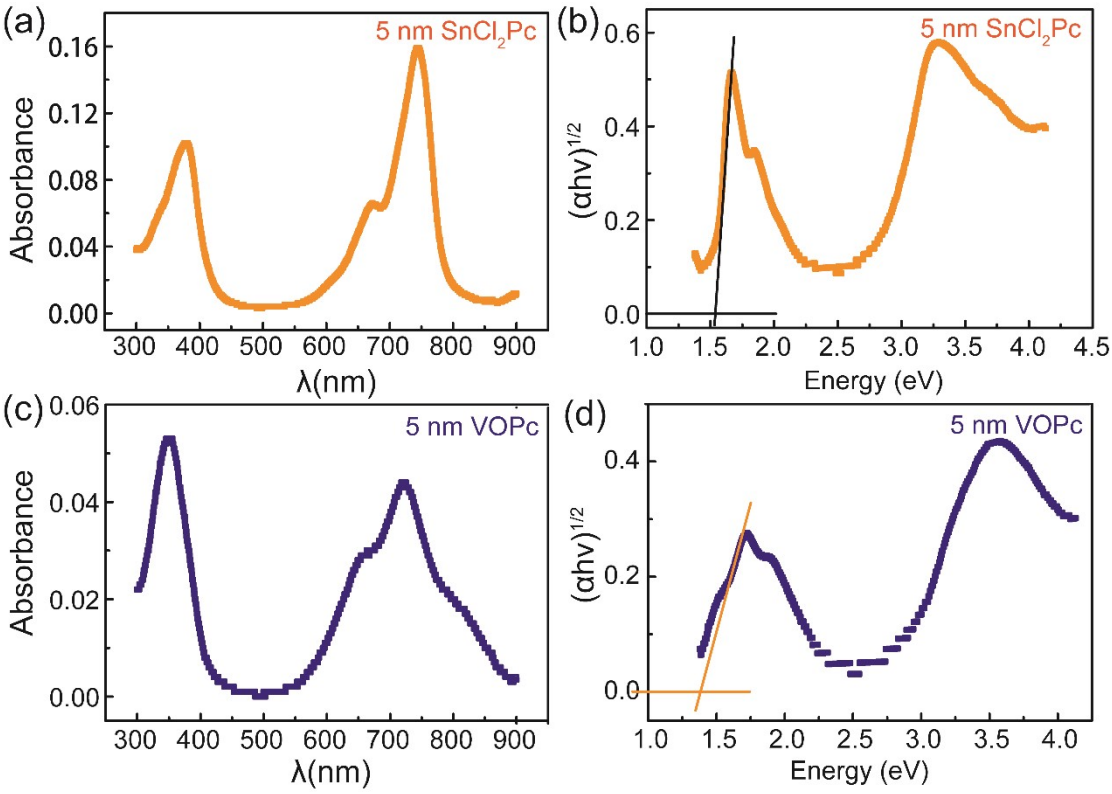

Figure S8. (a, b) UV-vis absorbance spectrum of VOPc and $SnCl_2Pc$ films, respectively and corresponding their tauc plots (c, d) of $(\alpha hv)^{1/2}$ as a function of energy based on $(\alpha hv)^{1/2}=C\ (hv-E_g)$, where α, h, v, C, and E_g are the absorption coefficient, Planck's constant, the incident light frequency, proportionality constant, and the band-gap energy, respectively.

To find out the optical band gap of VOPc film, we plot the UV-vis absorption spectrum of the VOPc film by using the Tauc equation.[1] Thus, bandgap energy (~1.41 eV) of the VOPc film is estimated from **Figure S8b**. Based on the UPS results (**Figure S7a, b**), the HOMO level of the VOPc film is determined to be about 5.12 eV. From the UPS results, we can get the Fermi energy (E_F) is around at 0.70 eV and the $E_{cut\text{-}off}$ is around at 16.8 eV. So we can calculate the E_{HOMO}: E_{HOMO} = 21.22 - (16.8-0.70) = 5.12 eV. From UV-vis and UPS measurements, we calculate the LUMO of VOPc film, about 3.71 eV, thus we calculate the HOMO/LUMO (5.12 eV/3.71 eV) energy levels of VOPc molecules. The HOMO/LUMO (5.41 eV/3.79 eV) energy level of $SnCl_2Pc$ molecules can also be calculated by the same method. [1, 2]

DFT predicted structure of MPc (M=VO, $SnCl_2$)/MoS_2 heterostructure

The geometry of VOPc and $SnCl_2Pc$ molecules on monolayer MoS_2 are predicted by geometry optimization calculation using PBE functional as implemented in VASP. The initial structure of MoS_2/MPc (M=VO, $SnCl_2$) was designed by minimizing the lattice mismatch between MoS_2 monolayer and organic molecules. The strain due to the lattice mismatch were applied to the organic layer. After that the atomic positions of constituents in the heterostructures were relaxed by the PBE functional as implemented in VASP. The structure of VOPc/MoS_2 and $SnCl_2Pc$/MoS_2 are relaxed to their minimum energy during the structural optimization. The orientations of the molecules with respect to MoS_2 in the molecule/MoS_2 heterostructure are depicted in Figure S9.

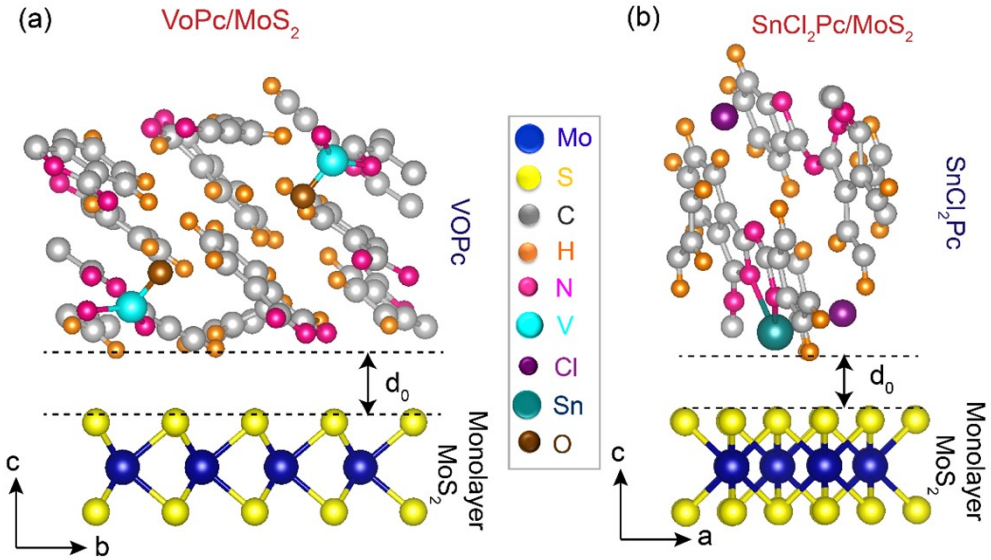

Figure S9. Optimized structure of (a) VOPc/MoS_2 (b) $SnCl_2Pc$/MoS_2 heterostructure. d_0 denotes the interlayer spacing between MoS_2 and organic layer.

State projected density of VOPc/MoS_2 heterostructure

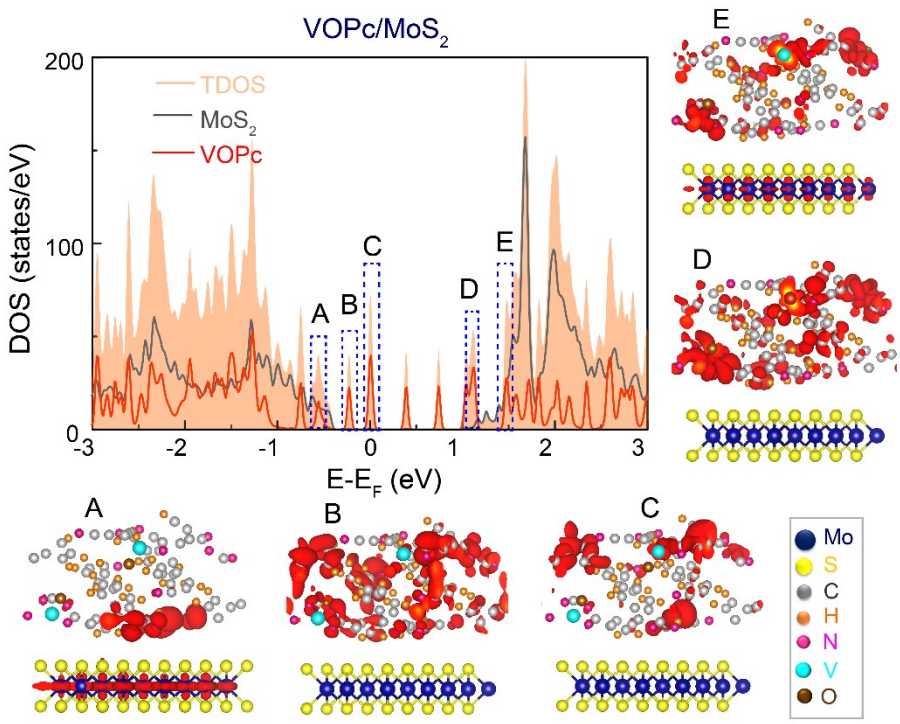

Figure S10. Density and projected density of states of VOPc/MoS2 heterostructure projected. A, B, and D, E represent the states below and above the Fermi level. The states at the Fermi level is denoted by C. The corresponding charge density for A, B, C, D and E states are depicted.

Effect of interlayer spacing on the density of states:

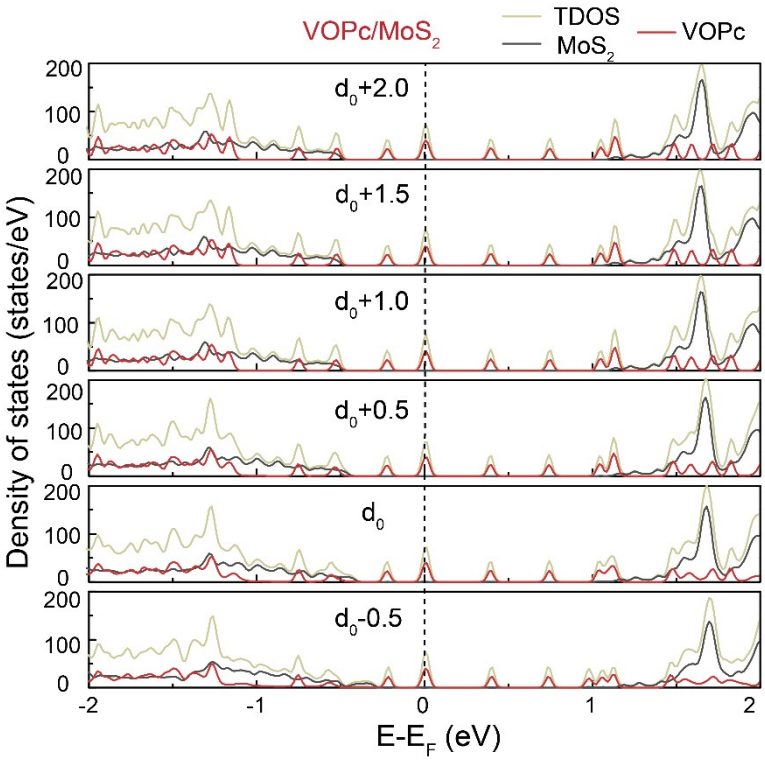

Figure S11. Variation of density of states with the interlayer spacing between MoS_2 and VOPc layer in VOPc/MoS_2 heterostructure. The equilibrium interlayer separation between MoS_2 and VOPc layer is d_0 Å.

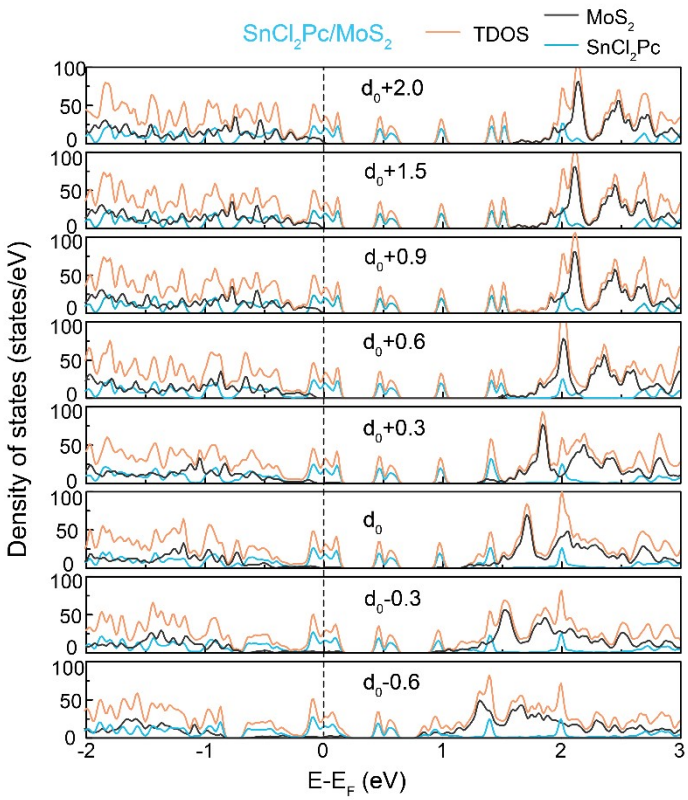

Figure S12. Variation of density of states with the interlayer spacing between MoS_2 and $SnCl_2Pc$ layer in $SnCl_2Pc/MoS_2$ heterostructure. The equilibrium interlayer separation between MoS_2 and $SnCl_2Pc$ layer is d_0 Å.

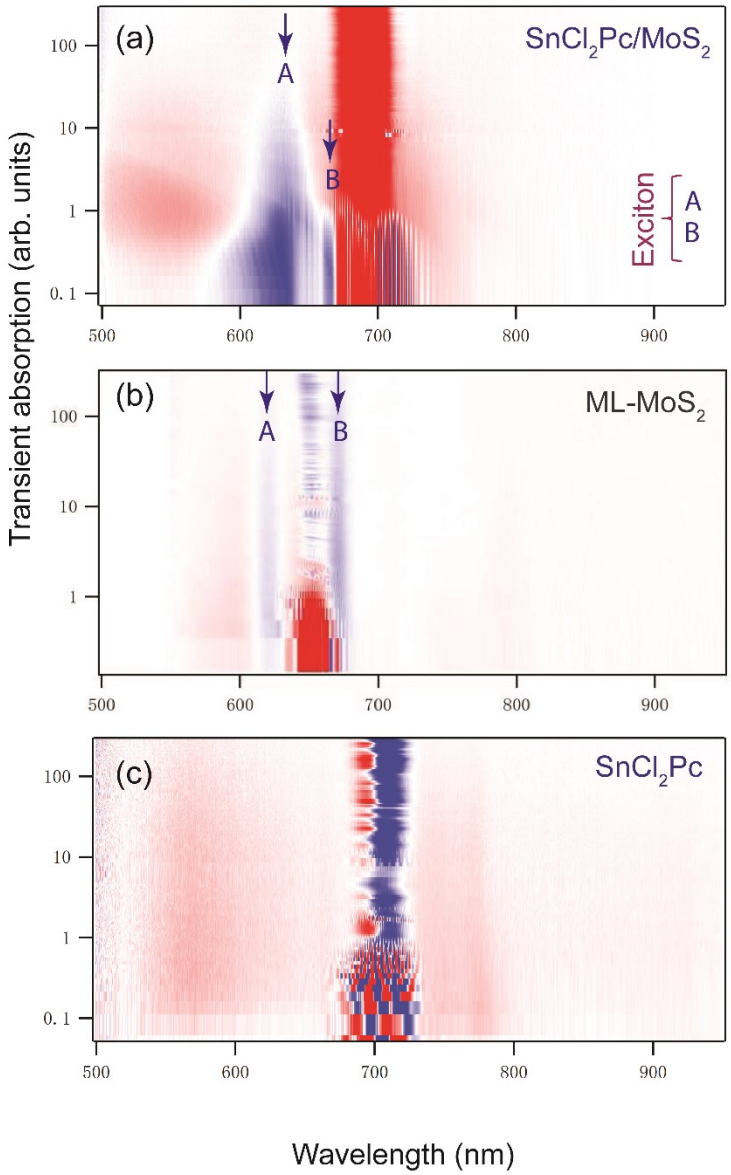

Figure S13. Transient absorption (a) $SnCl_2Pc/MoS_2$, (b) ML-MoS_2, and (c) $SnCl_2Pc$.

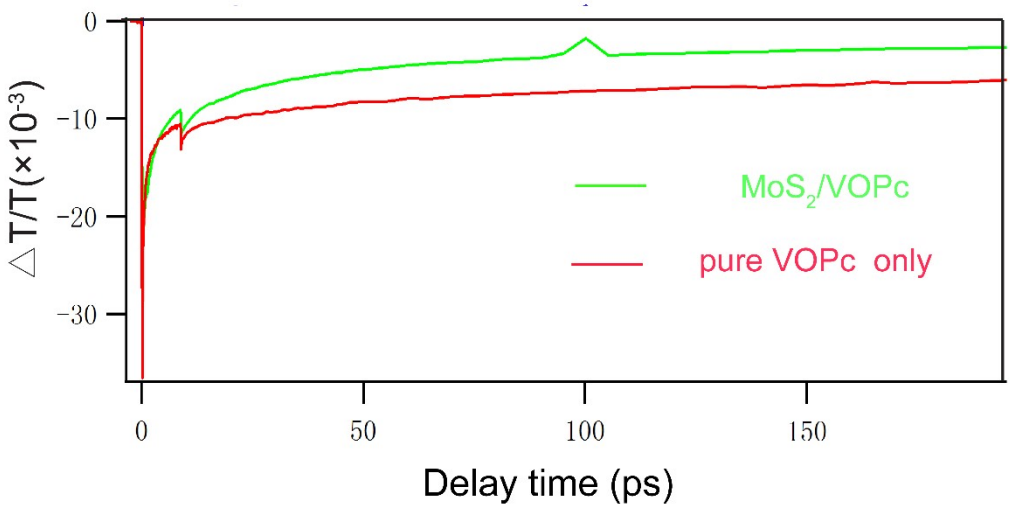

Figure S14. TA kinetics of the VOPc signal in MoS_2/VOPc heterostructure (green) and pure VOPc only (red), under 800 nm excitation. The results show that in the heterostructure, the decay of the signal became faster, indicating the existence of charge transfer from VOPc to MoS_2.

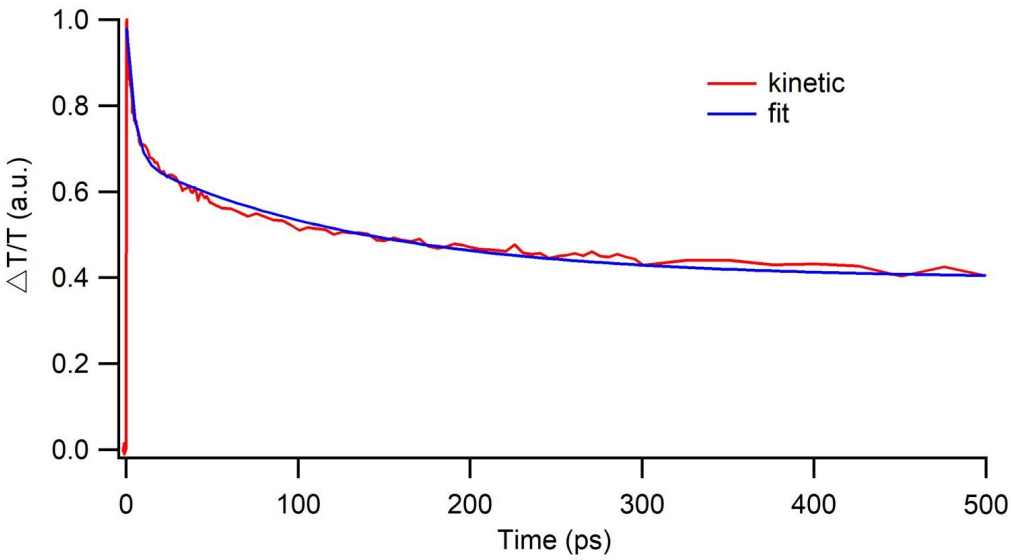

Figure S15. TA kinetics of the MoS_2 signal in MoS_2/VOPc heterostructure at 660 nm, under 800 nm excitation.

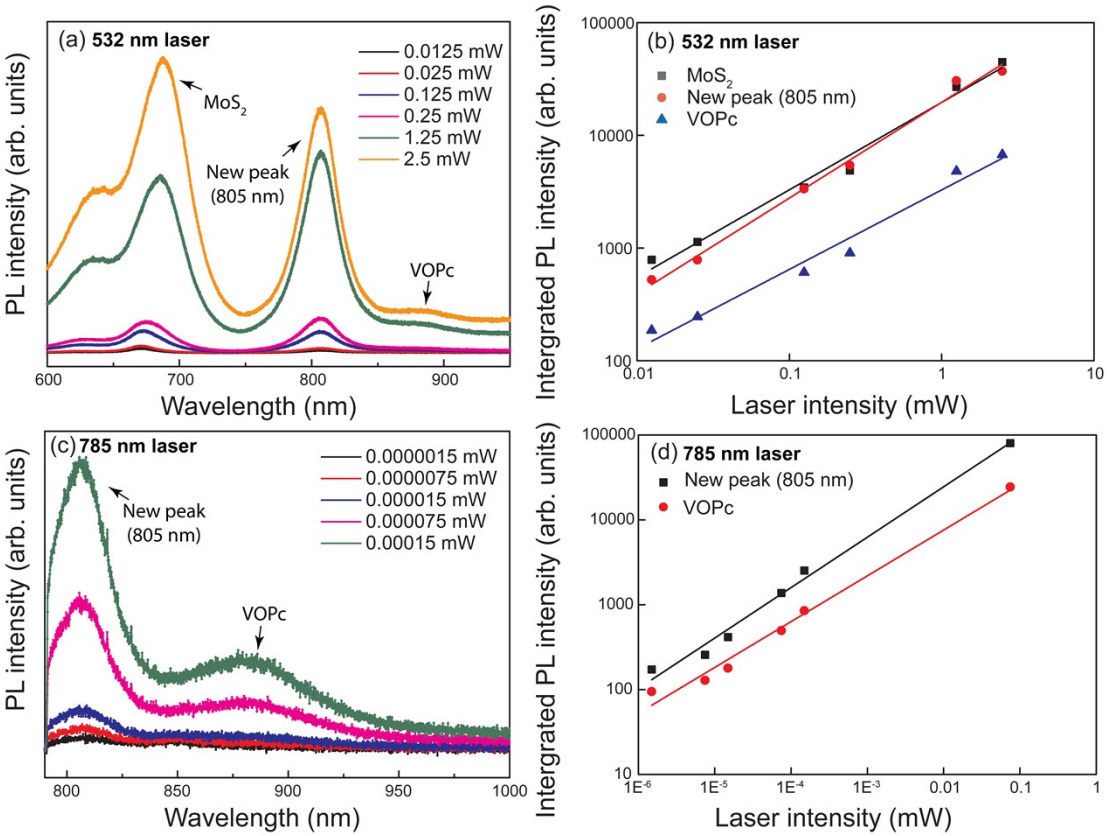

Figure S16. (a) PL spectra at the excitation wavelength of 532 nm and with varying excitation intensities. (b) Integrated PL intensity of MoS_2, NIR peak at 805 nm and VOPc as a function of the laser intensity plotted on a log–log scale for excitation at 532 nm. (c) PL spectra at the excitation wavelength of 785 nm and with varying excitation intensities. (b) Integrated PL intensity of NIR peak at 805 nm and VOPc as a function of the laser intensity plotted on a log–log scale for excitation at 785 nm.

PL measurements were made at room temperature using a Renishaw inVia Raman microscope using excitation wavelengths of 532 nm and 785 nm. The laser beam was focused on to the samples via a 50× objective lens producing a spot diameter of ~1 μm. The maximum laser power was kept at ~25 mW (532 nm) and 150 mW (785 nm) and it was varied using neutral density filters from 0.000001% to 100%.

We find that the PL intensity of MoS_2, new peak at 805 nm, and VOPc increases linearly with excitation power both under 532 nm and 785 nm laser beam. It is surprised that the PL intensity of MoS_2 excesses that of the new 805 nm when the excitation fluence is 2.5 mw. More studies are needed to understand the underlying mechanisms.

References

1. M. R. Habib, H. F. Li, Y. H. Kong, T. Liang, S. M. Obaidulla, S. Xie, S. P. Wang, X. Y. Ma, H. X. Su and M. S. Xu, *Nanoscale*, 2018, **10**, 16107-16115.
2. M. Ichikawa, S. Deguchi, T. Onoguchi, H. G. Jeon and G. D. Banoukepa, *Org Electron*, 2013, **14**, 464-468.
3. D. Kaplan, Y. Gong, K. Mills, V. Swaminathan, P. M. Ajayan, S. Shirodkar and E. Kaxiras, 2D Materials, 2016, 3, 015005.